Photochemistry of $[Ru(pytz)(btz)_2]^{2+}$ and characterisation of a κ^1-btz ligand-loss intermediate

Paul A. Scattergood, Usman Khushnood, Amina Tariq, David J. Cooke, Craig R. Rice and Paul I.P. Elliott*

Department of Chemistry, University of Huddersfield, Queensgate, Huddersfield, HD1 3DH, UK.

* corresponding author

p.i.elliott@hud.ac.uk

Abstract

We report the synthesis, characterisation and photochemical reactivity of the triazole-containing complex $[Ru(pytz)(btz)_2]^{2+}$ (**1**, pytz = 1-benzyl-4-(pyrid-2-yl)-1,2,3-triazole, btz = 1,1'-dibenzyl-4,4'-bi-1,2,3-triazolyl). The UV-visible absorption spectrum of **1** exhibits pytz- and btz-centred ^{1}MLCT bands at 365 and 300 nm respectively. Upon photo-excitation, acetonitrile solutions of **1** undergo conversion to the ligand loss intermediate, *trans*-$[Ru(pytz)(\kappa^2\text{-btz})(\kappa^1\text{-btz})(NCMe)]^{2+}$ (**2**, Φ_{363} = 0.013) and ultimately to the ligand loss product *trans*-$[Ru(pytz)(btz)(NCMe)_2]^{2+}$ (**3**), both of which are observed and characterised by ^{1}H NMR spectroscopy. Time-dependent density functional theory calculations reveal that the S_1 state of the complex has primarily HOMO→LUMO pytz-based ^{1}MLCT character. Data show that the ^{3}MLCT and ^{3}MC states are in close energetic proximity (≤ 0.11 eV to 2 d.p.) and that the T_1 state from a single point triplet state calculation at the S_0 geometry suggests ^{3}MC character. Optimisation of the T_1 state of the complex starting from the ground state geometry leads to elongation of the two Ru-N(btz) bonds *cis* to the pytz ligand to 2.539 and 2.544 Å leading to a psuedo 4-coordinate ^{3}MC state rather than the ^{3}MLCT state. The work therefore provides additional insights into the photophysical and photochemical properties of ruthenium triazole-containing complexes and their excited state dynamics.

Introduction

Thermally kinetically inert complexes of d^6 metals have received enormous interest in the literature over past decades due to their diverse applications in various fields of photophysics and photochemistry.[1] These range from light harvesting and solar energy conversion[2,3] to phosphorescent dopants in light emitting devices[4-8] for electronic display and artificial lighting applications. Significant efforts have therefore focused on the design of ligands for these complexes in order to maximise their light absorbing[9] and/or emissive properties.[10] The excited states in these complexes responsible for solar cell sensitisation or light emission, for example, are ^{3}MLCT states. Efficiency loss processes for phosphorescent emitters often involve higher-lying ^{3}MC states which, when in close enough energetic proximity, can be thermally populated from photoexcited ^{3}MLCT states.[11-13] These ^{3}MC states are also implicated in photochemical isomerisation and ligand ejection reactivity. Thus, modulation of the relative energies of ^{3}MLCT and ^{3}MC states through judicious ligand design can increase luminescent efficiency or conversely promote photochemical reactivity.

Whilst undesirable for light emitting applications, efforts to promote photochemical ligand ejection have recently attracted attention where complexes are desired as ruthenium(II)-based photoinitiated DNA binding agents in cancer therapy[14-16] or incorporated into molecular machines.[17,18] Typically, complexes are designed incorporating sterically encumbered ligands that weaken metal-ligand bonds and thus stabilise ^{3}MC states with respect to the ^{3}MLCT states when compared to complexes where such encumbrance is absent. This thereby increases the thermal accessibility of ^{3}MC states from photoexcited ^{3}MLCT states[19-25] (the terms *stabilisation* and *destabilisation* here refer to changes in the energies of these ^{3}MLCT and ^{3}MC states with respect to each other and the ground state when comparing complexes, for example, with the archetypical $[Ru(bpy)_3]^{2+}$. These energies can be determined or inferred spectroscopically, electrochemically and computationally and as $[Ru(N\hat{}N)_3]^{2+}$ complexes invariably have a highest occupied molecular orbital of predominantly metallic 4d character, and hence effectively the same ground state, these excited state energies can be readily compared). Work in our laboratory,[26-28] and those of others,[29-32] has shown that complexes containing 1,2,3-triazole rings that lack such steric promotion can also lead to photochemical reactivity, possibly through destabilisation of the ^{3}MLCT state with respect to the ^{3}MC state when compared to those states of the archetypal complex $[Ru(bpy)_3]^{2+}$. We recently reported the series of complexes $[Ru(bpy)_{3-n}(btz)_n]^{2+}$ (btz = 1,1'-dibenzyl-4,4'-bi-1,2,3-triazolyl, n = 1 to 3)[33] in which an increasing number of btz

ligands leads to destabilisation of the ^{1}MLCT bands in the visible absorption spectrum, significantly so for the homoleptic complex $[Ru(btz)_3]^{2+}$.[33-35] The heteroleptic complexes in this series were both shown to exhibit photochemical ejection of a btz ligand. In the case of $[Ru(bpy)_2(btz)]^{2+}$ in acetonitrile this results in the formation of the complex *cis*-$[Ru(bpy)_2(NCMe)_2]^{2+}$.[26] For $[Ru(bpy)(btz)_2]^{2+}$ this similarly results in the formation of a *bis*-solvento complex but occurs with concomitant ligand rearrangement to yield *trans*-$[Ru(bpy)(btz)(NCMe)_2]^{2+}$. Significantly, this is found to proceed with the rare[29,36-40] observation of a ligand loss intermediate, *trans*-$[Ru(bpy)(\kappa^2\text{-btz})(\kappa^1\text{-btz})(NCMe)]^{2+}$, containing a monodentate btz ligand which in this case shows unprecedented stability (Scheme 1).[27,28] Indeed, this intermediate species was crystallographically characterised.[25]

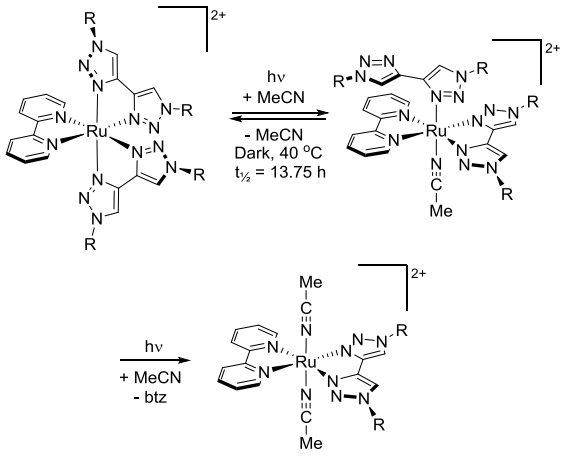

Scheme 1. Photochemical reactivity of the complex $[Ru(bpy)(btz)_2]^{2+}$ in acetonitrile (R = benzyl).

Density functional theory (DFT) calculations reveal that for the complexes in the series that contain bpy ligands that the lowest lying triplet excited state is a bpy-centred ^{3}MLCT state. However, for the homoleptic complex $[Ru(btz)_3]^{2+}$ the calculations suggest that the MLCT state destabilisation occurs to such an extent that the lowest singlet and triplet excited states become MC in character.[33] Intrigued by these results we decided to explore the photochemistry and photophysical properties of the complex $[Ru(pytz)(btz)_2]^{2+}$ (**1**) which contains five triazole rings. Here the pyridyltriazole, pytz, ligand is a hybrid of the bpy and btz ligands highlighted above. We therefore reasoned that this complex would enable us to explore the region of MLCT/MC state crossover as it would be expected to exhibit LUMO and MLCT state energies intermediate with respect to those of $[Ru(bpy)(btz)_2]^{2+}$ and $[Ru(btz)_3]^{2+}$. We therefore present here our recent results on the synthesis, characterisation and photochemical investigation of **1** and show that it undergoes similar photochemical

reactivity to $[Ru(bpy)(btz)_2]^{2+}$ in forming a ligand-loss intermediate with a monodentate btz ligand. We also present DFT calculations which show that whilst the S_1 state of the complex has ^{1}MLCT character the ^{3}MLCT and ^{3}MC are very close in energy facilitating population of the latter. This work therefore provides further insights into the fascinating photochemistry and photophysics imparted by this class of triazole-containing ligands.

Results & Discussion

The target complex **1** was prepared *via* a similar route to that previously reported for the synthesis of $[Ru(bpy)(btz)_2][PF_6]_2$ (Scheme 2).[33] Briefly, the pytz complex [Ru(*p*-cymene)(pytz)Cl][PF_6] was prepared by stirring a suspension of the dimer [Ru(*p*-cymene)$Cl_2]_2$ and pytz in methanol with isolation as its hexafluorophosphate salt. Though we had previously reported[41] its preparation we were slightly surprised to note that the structure of this relatively simple complex has not been published elsewhere. Crystals of X-ray diffraction quality were obtained from the slow vapour diffusion of diethyl ether into an acetonitrile solution of [Ru(*p*-cymene)(pytz)Cl]PF_6 . The structure of the cation is depicted in Figure 1 with selected bond lengths and angles listed in the caption.

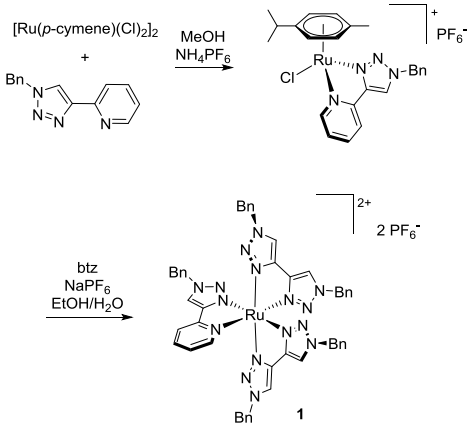

Scheme 2. Synthesis of $[Ru(pytz)(btz)_2][PF_6]_2$.

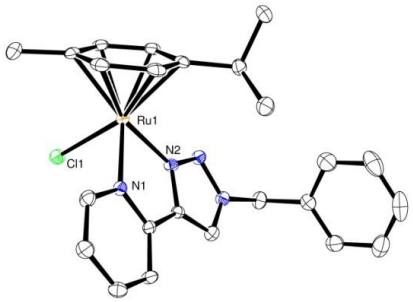

Figure 1. Molecular structure of the [Ru(*p*-cymene)(pytz)Cl]$^{+}$ cation. Counter ions, hydrogen atoms and co-crystallised solvent molecules are removed for clarity. All ellipsoids are shown at 50 % probability (Ru(1)-N(1) = 2.110(2), Ru(1)-N(2) = 2.078(2), Ru(1)-Cl(1) = 2.3849(7), N(1)-Ru(1)-N(2) = 76.46(8)**,** N(1)-Ru(1)-Cl(1) = 83.26(6), N(2)-Ru(1)-Cl(1) = 87.86(6)).

The complex crystallises in the P-1 space group along with one molecule of acetonitrile per ruthenium centre. The Ru centre is found to be in a distorted octahedral coordination environment if the arene is assumed to be pseudo-tripodal and exhibits a N(1)-Ru(1)-N(2) bite angle for the pytz ligand of 76.46(8) °. The bond-length between the metal centre and triazole nitrogen (Ru(1)-N(2), 2.078(2) Å) is comparable to that measured for similar complexes of ruthenium bearing triazole-containing ligands,[25] and is slightly shorter than the corresponding bond to the pyridine (Ru(1)-N(1), 2.110(2) Å). The torsion angle between planes defined by the pyridyl and triazole rings is 3.19 ° reflecting the essentially planar nature of the ligand. Analysis of the solid state packing structure shows evidence of favourable intermolecular π-π stacking interactions between the phenyl rings of the pytz ligand benzyl substituent.

Formation of **1** was achieved through reaction of [Ru(*p*-cymene)(pytz)Cl][PF_6] with two equivalents of btz in the presence of excess $NaPF_6$, yielding the product as a yellow powder. The downfield region of the ^{1}H NMR spectrum (d_3-MeCN) contains four near coincident singlet resonances (δ ~8.3) assigned to btz triazole ring protons which are all magnetically inequivalent due to the asymmetry of the pytz ligand. The triazole proton of the pytz ligand gives rise to a signal at δ 8.66 which has a strong nOe correlation with the resonance for the proximal proton at the 3-positon of the pyridine ring (δ 8.02). Further signals are observed at δ 7.95 and 7.86, assigned to the 4 and 6-positions of the pyridine ring respectively, with that corresponding to the 5-positon falling within the large multiplet for the benzylic phenyl resonances. In similar fashion to the signals for the triazole ring protons, the

lack of symmetry in the complex results in the five methylene groups of the benzylic substituents also being inequivalent. The signal for that of the pytz ligand appears at δ 5.58 ppm, with the remaining btz methylene protons giving rise to overlapping resonances between δ 5.53 and 5.56.

Crystals of X-ray diffraction quality were grown from the slow evaporation of an NMR sample of **1** and the resultant molecular structure is depicted in Figure 2. The asymmetric unit contains two crystallographically unique cations, both of which adopt a distorted octahedral geometry. The structure exhibits disorder in one of the phenyl rings of the benzyl substituent of one of the btz ligands of one of the cations. Disorder is also observed in one of the hexafluorophosphate counterions. This and the disorder in the cation were successfully modelled with partial occupancy. The Ru-N bond lengths are unremarkable and similarly to the structure of the cation [Ru(*p*-cymene)(pytz)(Cl)]$^{+}$, with the Ru-N(py) bonds being longer than the Ru-N(triazole) of the same ligand by 0.039 Å (Ru(1) cation) and 0.055 Å (Ru(2) cation).

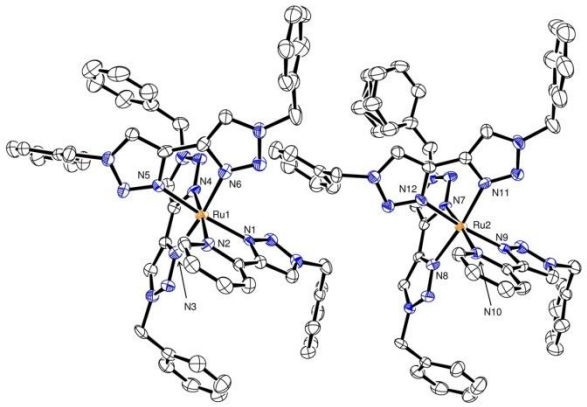

Figure 2. Structure of the asymmetric unit from the crystallographic data for $[Ru(pytz)(btz)_2][PF_6]_2$ (hydrogen atoms and hexafluorophosphate counterions removed for clarity). Ellipsoids shown at 50 % probability (Ru(1)-N(1) = 2.055(5), Ru(1)-N(2) = 2.094(5), Ru(1)-N(3) = 2.071(5), Ru(1)-N(4) = 2.060(5), Ru(1)-N(5) = 2.055(5), Ru(1)-N(6) = 2.042(5), Ru(2)-N(7) = 2.073(4), Ru(2)-N(8) = 2.072(5), Ru(2)-N(9) = 2.036(5), Ru(2)-N(10) = 2.091(5), Ru(2)-N(11) = 2.046(5), Ru(2)-N(12) = 2.056(5)).

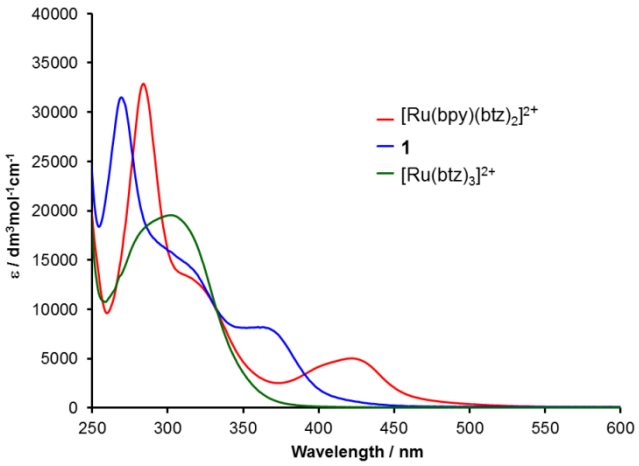

Figure 3. UV-Visible absorption spectra for acetonitrile solutions of **1**, $[Ru(bpy)(btz)_2]^{2+}$ and $[Ru(btz)_3]^{2+}$.

UV-Visible absorption spectra of an acetonitrile solution of **1** and those of its close analogues $[Ru(bpy)(btz)_2]^{2+}$ and $[Ru(btz)_3]^{2+}$, are shown in Figure 3. The spectrum of **1** exhibits a broad band centred at around 365 nm assigned to a metal-to-ligand charge transfer (^{1}MLCT) transition involving the pytz ligand. This band is positioned mid-way between the bpy-based ^{1}MLCT band for $[Ru(bpy)(btz)_2]^{2+}$ (420 nm) and the btz-based ^{1}MLCT absorption at around 300 nm for $[Ru(btz)_3]^{2+}$. Since the LUMO of btz is calculated to be significantly higher in energy than that of bpy (by ~ 1 eV)[33] then the LUMO of the hybrid of these two ligands, pytz, would be expected to be intermediate in energy[42] thus leading to the observed significant blue-shift in the ^{1}MLCT band compared to that of $[Ru(bpy)(btz)_2]^{2+}$. The spectrum of **1** also exhibits an intense band at 270 nm assigned to ligand-centred $\pi\rightarrow\pi^*$ transitions which shows a large shoulder at 320 nm assigned to btz-centred ^{1}MLCT transitions. This is supported by the position of a similar shoulder for $[Ru(bpy)(btz)_2]^{2+}$ and the absorption maximum observed in this region for $[Ru(btz)_3]^{2+}$.

Unlike $[Ru(bpy)(btz)_2]^{2+}$, which is emissive at low temperature in frozen solution,[33] no discernible emission was observed for **1** in either room temperature MeCN solutions nor at 77 K in a 4:1 EtOH:MeOH solvent glass (Supporting Information, Figure S7). The quenching of emission for **1** is therefore likely to be due to the population of non-emissive ^{3}MC states from an elevated ^{3}MLCT level. The latter state is destabilised relative to that of $[Ru(bpy)(btz)_2]^{2+}$ due to the substitution of bpy for pytz and the resultant raising in energy of the LUMO. The absence of emission for **1** is indicative of efficient depopulation of the ^{3}MLCT state, suggesting that this level lies at least very close in energy to that of the ^{3}MC

state. Consistent with our previous work, $[Ru(btz)_3]^{2+}$ was also found to be non-emissive at both room temperature and 77 K.[33]

Electrochemical analysis of **1** in dichloromethane reveals one reversible oxidation process within the potential range +1.8 to -2.0 V vs Fc^+/Fc (see Supporting Information, Figure S4). This process is attributed to the one-electron Ru(II)/Ru(III) oxidation, with a half-potential of +0.98 V and is consistent with those reported for $[Ru(bpy)(btz)_2]^{2+}$ and $[Ru(btz)_3]^{2+}$ (+0.98 and +1.01 V respectively).[33] It may therefore be concluded that the HOMO is localised predominantly on the Ru centre, in good agreement with DFT computational calculations (*vide infra*). It is noted that no ligand-centred reduction processes were observed. As these would be anticipated to occur at a more cathodic potential than that for the reduction of $[Ru(bpy)(btz)_2]^{2+}$, for which no clear reduction processes were identified,[33] it is assumed that reductions for **1** similarly lie beyond the lower limit of the electrochemical solvent window.

To probe the photochemical reactivity of **1**, acetonitrile solutions of **1** were subject to irradiation utilising a 23 W fluorescent lamp (the output profile of which is shown in the Supporting Information, Figure S6) and monitored by both ^1H NMR and UV-visible absorption spectroscopy. ^1H NMR spectra of **1** during photolysis in d_3-acetonitrile are shown in Figure 4.

As the photolysis of **1** progresses, signals for a second complex *trans*-[Ru(pytz)(κ^2-btz)(κ^1-btz)(NCMe)]$^{2+}$ (**2**, Scheme 3), are observed to grow in intensity. In similar fashion to spectra recorded during the photolysis of $[Ru(bpy)(btz)_2]^{2+}$ [27,28] a doublet resonance corresponding to the pyridine 6-position is observed at δ 10.03 with further resonances observed and confirmed by $^1H^1H$-COSY spectroscopy for the 3-, 4- and 5-positions at δ 7.79, 7.97 and 7.51 respectively. The triazole proton of the pytz ligand gives rise to a singlet resonance at δ 8.43. The bidentate btz ligand exhibits triazole ring proton resonances at δ 8.25 and 8.19. The $^1H^1H$-NOESY spectrum reveals that the resonances for one of the methylene groups of this κ^2-btz ligand along with that of the pytz ligand appear as the overlapping multiplet between δ 5.60 and 5.64. The second methylene group of this κ^2-btz ligand gives rise to a diastereotopic pair of roofed doublets centred at δ 5.82 (J_{HH} = 14.9 Hz). The κ^1-btz ligand gives rise to methylene resonances at δ 5.36 and 5.08 which exhibit nOe interactions with resonances for the protons of the triazole rings to which they are attached at δ 7.27 and 7.64 respectively. The latter of these methylene groups appears as a diastereotopic

pair of roofed doublets (J_{HH} = 14.7 Hz) due to the asymmetry of the plane defined by the pytz and κ^2-btz ligands. The inner lines of these doublets are almost coincident, with the outer lines only just evident. These signals also give rise to a nOe interaction with the *ortho* protons of a phenyl ring (δ 6.87) which is well resolved. The well resolved nature of this phenyl resonance presumably arises from proximity of the phenyl ring to the coplanar bidentate ligands suggesting that the triazole ring to which this benzyl substituent is attached is the one coordinated to the metal.

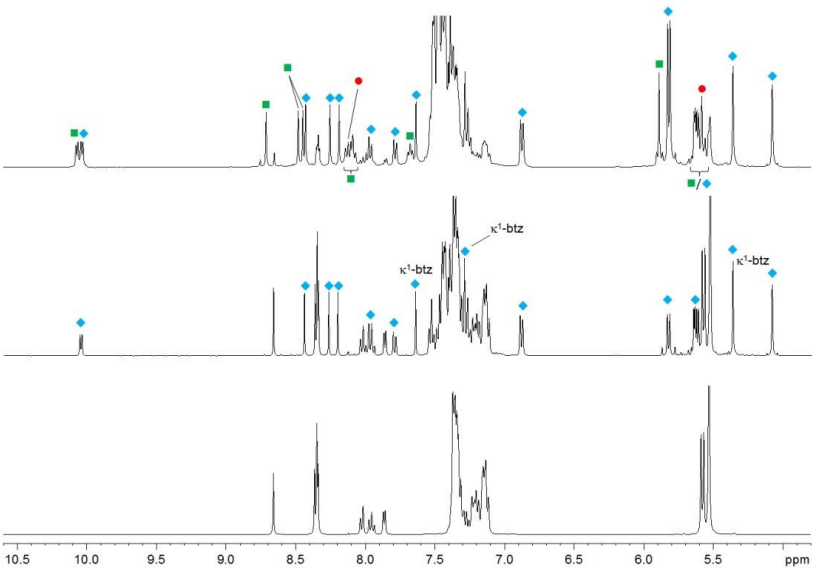

Figure 4. ^{1}H NMR spectra recorded during the photolysis of **1** in d_3-acetonitrile (bottom: initial spectrum, middle: 2 hours irradiation, top: 9 days irradiation. ♦ = **2**, ■ = **3**, ● = free btz).

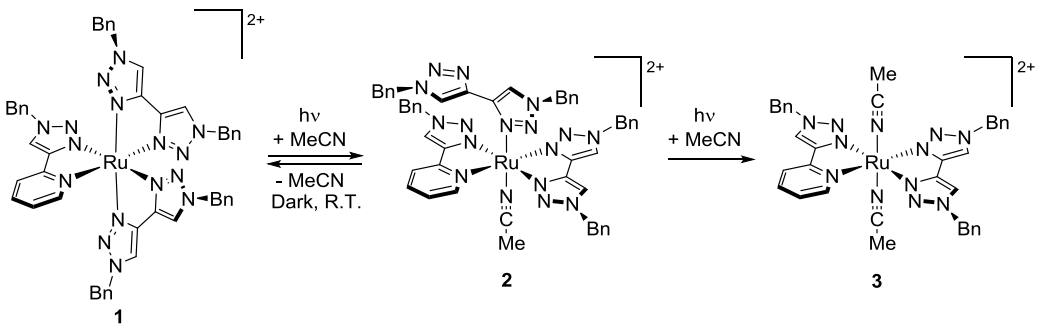

Scheme 3. Photochemical reactivity of [Ru(pytz)(btz)$_2$]$^{2+}$ (**1**) in acetonitrile to yield *trans*-[Ru(pytz)(κ^2-btz)(κ^1-btz)(NCMe)]$^{2+}$ (**2**) and *trans*-[Ru(pytz)(btz)(NCMe)$_2$]$^{2+}$ (**3**).

Due to the striking similarity of the resonances in these spectra to those previously observed for *trans*-[Ru(bpy)(κ^2-btz)(κ^1-btz)(NCMe)]$^{2+}$ [27,28] we can be confident in our assignment of the structure of **2** as *trans*-[Ru(pytz)(κ^2-btz)(κ^1-btz)(NCMe)]$^{2+}$. This is despite the fact that all five triazole rings will be inequivalent in either the possible *cis* or *trans* isomers. This stereochemical assignment is further supported by the relative stability of **2** toward rechelation of the monodentate btz ligand which arises in *trans*-[Ru(bpy)(κ^2-btz)(κ^1-btz)(NCMe)]$^{2+}$ due to the lack of a labile *cis* solvent ligand. Electrospray mass spectrometry analysis of NMR samples in d_3-acetonitrile undergoing photolysis reveal the presence of a dication corresponding to **2** exhibiting the expected isotope pattern for a ruthenium complex (m/z 507.16 for ^{102}Ru, Supporting Information, Figure S5). When a partly photolysed sample of **1** exhibiting resonances for **2** is left in the dark over 2 days reversion to the starting material is observed. Several attempts were made to grow crystals of the photo-product for X-ray diffraction but these were unsuccessful.

After prolonged irradiation, further resonances are observed for the photolysis product **3**. Resonances for the pytz pyridine ring are observed at δ 10.07, 7.67, 8.12 and 8.08 with that for the triazole ring proton of the same ligand appearing as a singlet at δ 8.71. The inequivalent triazole protons of the btz ligand give rise to two singlets at δ 8.48 and 8.45. Methylene resonances for **3** are observed at δ 5.89 and overlapping with resonances for **2** at δ 5.60 to 5.64. Again, by analogy to the photolysis observed for [Ru(bpy)(btz)$_2$]$^{2+}$ we assign the structure of **3** as *trans*-[Ru(pytz)(btz)(NCMe)$_2$]$^{2+}$. Electrospray mass spectrometry analysis of NMR samples in d_3-acetonitrile show the presence of the dication **3** and also the monocationic ion pair {[Ru(pytz)(btz)(NCCD$_3$)$_2$][PF$_6$]}$^+$ (for ^{102}Ru, m/z 371.12 and 887.21 respectively, Supporting Information, Figure S5) Characteristic resonances corresponding to free btz (δ 8.12 and 5.59) are also discernable as signals for **3** are observed to grow.

UV-visible absorption spectra recorded over a five minute period during the photolysis of an optically dilute acetonitrile solution of **1** (Figure 5) show a slight bleaching and red-shift in the $\pi \rightarrow \pi^*$ band at 270 nm and a more significant bleaching of the btz-centred ^{1}MLCT band at 320 nm consistent with the dechelation of one of the btz ligands. A similar bleaching of the btz-based ^{1}MLCT band is observed during the photolysis of [Ru(bpy)(btz)$_2$]$^{2+}$.[27] This is accompanied by a small red-shift of the pytz-centred ^{1}MLCT band by approximately 4 nm. ^{1}H NMR analysis of the irradiated solution upon reaching a stationary point in the UV-Visible absorption spectra reveals the dominant species present to

be *trans*-[Ru(pytz)(κ^2-btz)(κ^1-btz)(NCMe)]$^{2+}$, indicating that the initial rapid change in electronic absorption (Figure 5) corresponds to the dechelation of btz and formation of the mono-solvento photo-product. The reaction is rather slow when compared to that of [Ru(bpy)(btz)$_2$]$^{2+}$ carried out under identical conditions. Complex **1** is observed to be still undergoing conversion to **2** after 3 minutes whereas conversion of [Ru(bpy)(btz)$_2$]$^{2+}$ to its corresponding κ^1-btz intermediate is essentially complete in 60 seconds (Supporting Information, Figure S6). This might be surprising given the observed destabilisation of the ^{1}MLCT state of **1** relative to that of the latter. This would be expected to make ^{3}MC state population far more facile and hence make the complex more reactive. However, the blue-shift in the ^{1}MLCT band, which only just encroaches into the visible spectrum, means that there will be a significantly diminished absorption overlap with the emission profile of the light source. Indeed, **1** is almost exclusively excited by the emission line of the lamp at 363 nm, whereas the absorption profile of [Ru(bpy)(btz)$_2$]$^{2+}$ overlaps with additional, more intense excitation lines at 404 and 435 nm (see Supporting Information, Figure S6).

Utilising exclusively an excitation wavelength of 363 nm and a ferrioxalate chemical actinometer, the quantum yield of the first photodechelation step was estimated to be Φ_{363} = 0.013. The magnitude of this quantum yield is noted to be similar to that reported recently for the photo-induced ejection of pyridine from a ruthenium(II) *tris*(2-pyridylmethyl)amine (TPA)-containing complex.[43] Likewise, the yield of photo-product formation is consistent with that of Ru(II) complexes featuring 1,2,3-triazole-containing variants of the TPA moiety, where an arm of the tripodal ligand is replaced by a solvent molecule upon irradiation.[44] In these systems it has been found that fully triazolated TPA analogues used in conjunction with 2,2'-bipyridine give rise to photo-product quantum yields of similar magnitude to ($\Phi_{350\text{-}400}$ = 0.036, Φ_{436} = 0.0604), though greater than that measured here for **1**.

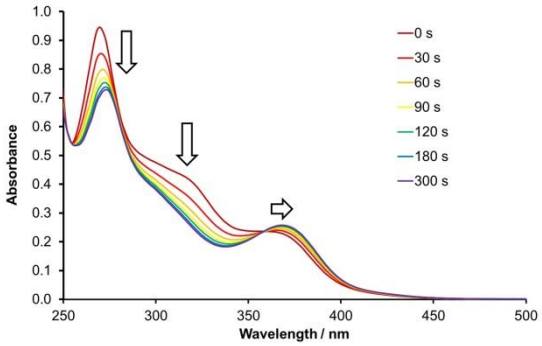

Figure 5. UV-Visible electronic absorption spectra recorded during the photolysis of **1** in acetonitrile. Times shown correspond to cumulative irradiation.

In order to more fully understand the photophysical properties of **1** we turned to DFT calculations. The ground state geometry of **1** was optimised at the B3LYP level of theory using the Stuttgart-Dresden ECP for ruthenium and 6-311G* basis sets for all other atoms. In order to reduce the computational cost the benzyl substituents of the pytz and btz ligands were simplified to methyl substituents. The calculated structure of the complex displays a distorted octahedral geometry, key structural parameters for which are provided in Figure 6. The longest Ru-N bond length is the Ru-N(py) bond (2.125 Å) with the Ru-N(tz) bond lengths shorter at an average of 2.091 Å. The shortest of these is the Ru-N(tz) bond for the pytz ligand (2.064 Å) which results in an elongation of the Ru-N(tz) bond *trans* to it (2.108 Å). The relative trend in these calculated Ru-N bond lengths is consistent with those measured through X-ray crystallography (*vide supra*).

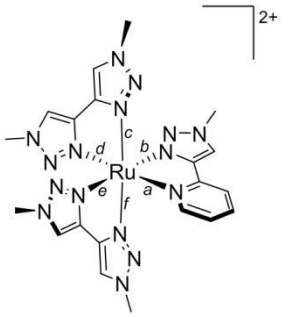

Ru-N	S_0	T_1
a	2.125	2.138
b	2.064	2.076
c	2.094	**2.539**
d	2.098	2.143
e	2.108	2.149
f	2.093	**2.544**

Figure 6. Calculated bond lengths for the optimised ground state and triplet excited state of **1** (elongated Ru-N bonds for the T_1 state in bold).

The frontier molecular orbital isosurfaces for **1** were plotted (Figure 7 and Table S1, Supporting Information) and the energies of these orbitals determined. The relative energies of the molecular orbitals for **1**, with comparison to those of $[Ru(bpy)(btz)_2]^{2+}$ and $[Ru(btz)_3]^{2+}$, are depicted in Figure 8. The HOMO has purely metallic $4d_{z^2}$ character as would be expected for a pseudo-C_3 symmetric $[Ru(N\text{^}N)_3]^{2+}$-type complex[45,46] and resides at -10.74 eV (2 d.p.), nearly isoenergetic with those of $[Ru(bpy)(btz)_2]^{2+}$ and $[Ru(btz)_3]^{2+}$ (-10.83 and -10.64 eV respectively). The LUMO is primarily localised on the pyridine ring of the pytz ligand with an additional lesser contribution from the triazole ring of the same ligand. Residing at -6.64 eV (2 d.p.) this is mid-way between the LUMO of $[Ru(bpy)(btz)_2]^{2+}$ (-7.09 eV) and $[Ru(btz)_3]^{2+}$ (-5.95 eV), as might be expected, and results in the HOMO-LUMO energy gap of 4.11 eV (to 2 d.p.). This data reflects the observed position of the ^{1}MLCT

electronic absorption band for **1** at a point straddled by those of $[Ru(bpy)(btz)_2]^{2+}$ and $[Ru(btz)_3]^{2+}$. The Ru-N anti-bonding dσ* orbitals for the ground state of **1** are LUMO+9 and LUMO+10 and appear at -4.87 and -4.77 eV and are close in energy to those of $[Ru(btz)_3]^{2+}$ (LUMO+9 -4.68 eV). The narrowing of the gap between the LUMO and the dσ* orbitals for **1** (1.77 eV) relative to the comparable gap for $[Ru(bpy)(btz)_2]^{2+}$ (2.15 eV) would therefore suggest a closer proximity of the MLCT and MC excited states of the complex.

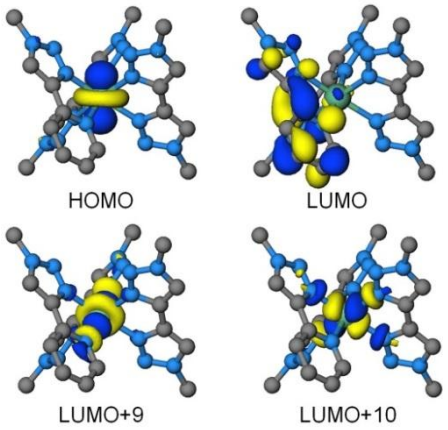

Figure 7. Plots of the HOMO and LUMO molecular orbitals of **1** along with plots of the dσ* LUMO+9 and LUMO+10 orbitals.

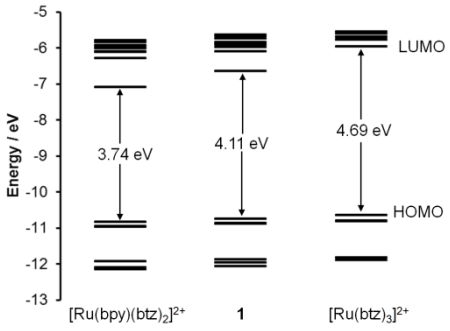

Figure 8. Molecular orbital energy level diagram for complex **1** with those of $[Ru(bpy)(btz)_2]^{2+}$ and $[Ru(btz)_3]^{2+}$ for comparison (HOMO – LUMO gaps quoted to 2 d.p.).

A time-dependent DFT calculation was carried out at the ground state geometry of **1** to simulate the optical absorption spectrum of the complex (Figure 9). The energies of the lowest 50 singlet vertical excitations were calculated and the character of the major transitions determined (Table 1). Whilst the energies of the major transitions appear slightly

overestimated they are in fairly good agreement with the experimental data. The S_1 state calculated at 388 nm is of HOMO→LUMO ^{1}MLCT character but is of very low oscillator strength and will therefore contribute little to the observed spectrum. The first major transition, corresponding to excitation to the S_3 state, is at 351 nm and is of mixed HOMO-1→LUMO and HOMO-2→LUMO ^{1}MLCT character with charge-transfer to the pytz ligand. This transition is blue-shifted by 35 nm relative the comparable first intense transition calculated for $[Ru(bpy)(btz)_2]^{2+}$ (S_3, 386 nm)[33] and clearly matches the experimentally observed blue-shift in the ^{1}MLCT band. Several intense transitions between 282 and 309 nm are of primarily ^{1}MLCT character with charge-transfer to btz. This is in agreement with the assignment of the shoulder at approximately 300 nm in the experimentally recorded UV-visible absorption spectrum of **1** and calculations previously reported for $[Ru(bpy)_2(btz)]^{2+}$ and $[Ru(bpy)(btz)_2]^{2+}$.[33] The excitations centred at 255 nm of high oscillator strength are assigned as pytz- and btz-centred $\pi\rightarrow\pi^*$ transitions.

Since the lowest singlet excited state of $[Ru(btz)_3]^{2+}$ was previously calculated to have ^{1}MC character we expected the elevated LUMO of **1** relative to that of $[Ru(bpy)(btz)_2]^{2+}$ to result in closer proximity of the ^{1}MLCT and ^{1}MC states. Examination of the minor components to the three lowest energy calculated singlet states reveal contributions involving population of the $d\sigma^*$ orbitals (coefficients $\geq$ 0.1). The first states with significant ^{1}MC character, however, are S_4 (340 nm) and S_5 (337nm) which lie 0.45 and 0.48 eV above the S_1 state. Both of these transitions have low oscillator strengths of 0.0031 and 0.00094 respectively. Whilst the dominant contribution to the S_4 state has HOMO→LUMO+2 (35 %) ^{1}MLCT character there are is also a significant ^{1}MC based contribution resulting from a HOMO→LUMO+10 (18 %) transition. The S_5 state is dominated by ^{1}MC character with the two most significant contributions being HOMO→LUMO+9 (47 %) and HOMO-2→LUMO+9 (16 %) with other lesser contributing transitions involving population of the second $d\sigma^*$ (LUMO+10) orbital. The real energy barrier connecting the ^{1}MLCT and ^{1}MC states along the singlet excited state potential energy surface will obviously be far smaller than the S_1-S_4 and S_1-S_5 vertical energy separations quoted above which would represent the upper limit.

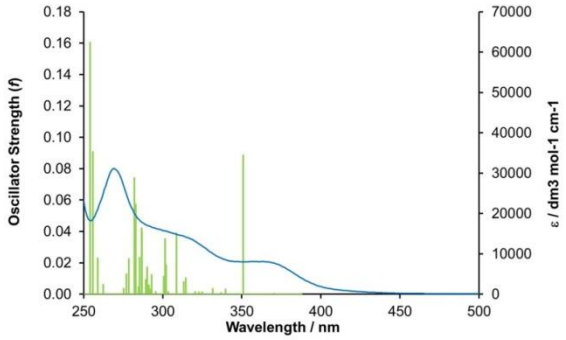

Figure 9. TDDFT calculated absorption spectrum for **1** (experimental absorption spectrum overlaid).

Table 1. Wavelengths, energies, oscillator strengths (*f*), predominant composition and character for selected singlet excitations from the TDDFT calculated UV-visible absorption spectrum of **1**. Energies, compositions and character of the two lowest energy triplet excitations from the singlet ground state wavefunction are also listed.

Transition	λ / nm	Energy / eV (*f*)	Composition	
S_1	388	3.20 (0.00052)	HOMO→LUMO	^{1}MLCT(pytz)
S_3	351	3.53 (0.0885)	HOMO-2→LUMO HOMO-1→LUMO	^{1}MLCT(pytz)
S_4	340	3.65 (0.0031)	HOMO→LUMO+2 HOMO→LUMO+1 HOMO→LUMO+10	^{1}MLCT(pytz & btz)/ ^{1}MC
S_5	337	3.68 (0.00094)	HOMO→LUMO+9 HOMO-2→LUMO+9	^{1}MC
S_{12}	309	4.02 (0.0388)	HOMO-1→LUMO+1 HOMO-2→LUMO+4	^{1}MLCT(pytz & btz)
S_{15}	302	4.11 (0.0352)	HOMO-2→LUMO+1 HOMO-2→LUMO+2	^{1}MLCT(pytz & btz)
S_{23}	287	4.32 (0.0399)	HOMO-1→LUMO+6 HOMO-1→LUMO+4 HOMO-1→LUMO+5 HOMO→LUMO+8	^{1}MLCT(pytz & btz)
S_{24}	287	4.33 (0.0422)	HOMO-1→LUMO+7	^{1}MLCT(pytz)
S_{27}	283	4.38 (0.0574)	HOMO-2→LUMO+6 HOMO-2→LUMO+5	^{1}MLCT(pytz & btz)

S_{28}	282	4.39 (0.0740)	HOMO-1→LUMO+7 HOMO-1→LUMO+6	^{1}MLCT(pytz & btz)
S_{35}	256	4.85 (0.0906)	HOMO-5→LUMO HOMO-3→LUMO	^{1}LC
S_{36}	254	4.87 (0.160)	HOMO-5→LUMO HOMO-3→LUMO	^{1}LC
T_1		2.97	HOMO→LUMO	^{3}MLCT(pytz)
T_2		3.09	HOMO→LUMO+9	^{3}MC

The energies of the lowest triplet excited states were also determined by a TDDFT calculation for the ground state optimised geometry and singlet ground state wavefunction and reveal that the T_1 state lies 2.97 eV above the ground state and is of HOMO→LUMO ^{3}MLCT character. However, the T_2 state, which lies only 0.11 eV (to 2 d.p.) higher in energy, is of predominantly HOMO→LUMO+9 ^{3}MC character (Table 1).

The energy of the lowest triplet excited state was alternatively calculated in a single-point SCF calculation at the ground state geometry using the constraint of the spin multiplicity of 3. This therefore effectively calculates the triplet electronic *ground* state at this geometry and hence is representative of the T_1 state after its formation and is calculated to lie 3.09 eV above S_0. A plot of the spin density (Figure 10a) shows that the unpaired electrons are localised primarily at the metal centre indicating ^{3}MC character. A triplet TDDFT calculation after this single-point calculation allows the determination of the energies of higher lying triplet excited states.[45,46] The first root determined from this calculation, and therefore the T_2 state, lies only very slightly higher in energy by 0.017 eV. This is dominated by a transition of an electron in the higher-energy singly-occupied molecular orbital to the LUMO which is localised on the pyridyl ring and is therefore of ^{3}MLCT character. Since solvation might be expected to stabilise ^{3}MLCT states whilst leaving ^{3}MC comparatively unperturbed, the single-point triplet calculation was repeated using the COSMO solvation model[47] with acetonitrile as the solvent (ε = 37.5). Even with the solvent model applied the spin density plot still indicates a ^{3}MC state.

This T_1 state was allowed to optimise with a triplet spin multiplicity. As the geometry relaxes the two mutually *trans* Ru-N(btz) bonds *cis* to the pytz ligand, labelled *c* and *f* in Figure 6, are observed to significantly elongate to 2.539 and 2.544 Å respectively, again indicative of the ^{3}MC state character (Figure 10b). This structure is in agreement with those previously calculated and reported for ^{3}MC states in Ru(II) *tris*(diimine) complexes by Alary and co-workers[45,46] and the T_1 state of $[Ru(btz)_3]^{2+}$.[33] A plot of the spin density again reveals that the unpaired electrons are primarily localised on the ruthenium centre confirming the ^{3}MC character of this T_1 state.

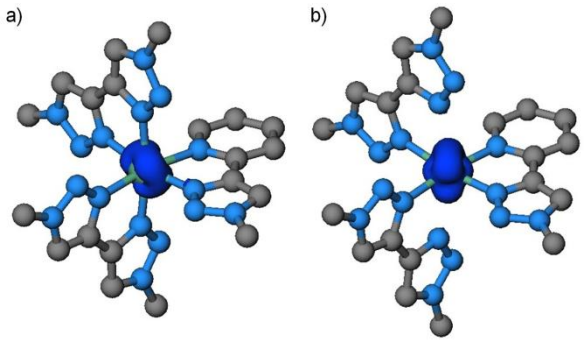

Figure 10. a) spin density for a single-point DFT calculation at the ground state geometry of **1** with a triplet spin multiplicity, b) structure and spin density for the optimised T_1 state of **1**.

The TDDFT data for triplet excitations from the singlet ground state wavefunction and the triplet state wavefunction single-point calculations at the same geometry above would appear to give contradictory results as to the nature of the lowest energy triplet excited state. However, the triplet TDDFT states calculated are a superposition of possible transitions from the singlet ground state whereas the triplet single-point calculation determines the electronic distribution of the *triplet ground state* at that geometry. For excited states that lie close in energy to one another it might well be expected that the relative ordering of the states from these calculations might not necessarily be in agreement. Nevertheless, the results clearly show that the ^{3}MLCT and ^{3}MC states are indeed very close in energy and thus the latter will inevitably be efficiently populated leading to the observed photochemical reactivity.

Conclusions

We have prepared and characterised the complex $[Ru(pytz)(btz)_2]^{2+}$ containing five 1,2,3-triazole coordinating moieties and investigated its photophysical and photochemical properties. The complex undergoes light-activated ligand ejection *via* the observed ligand loss intermediate *trans*-$[Ru(pytz)(\kappa^2\text{-btz})(\kappa^1\text{-btz})(NCMe)]^{2+}$ mirroring photochemical behaviour of previously reported ruthenium bitriazolyl complexes. Computational investigations show that the complex exhibits ^{3}MLCT and ^{3}MC states that are very close in energy facilitating the efficient population of the latter and accounting for the photochemical reactivity observed. Indeed, a single-point calculation at the ground state geometry with a triplet spin multiplicity reveals ^{3}MC state character. This complex adds further insights into the fascinating photochemistry imparted by triazole-based ligands and allows us to probe the region of MLCT/MC state crossover. Further theoretical investigations on these systems are ongoing and results will be published in due course.

Acknowledgements

The authors thank the University of Huddersfield for supporting this research. As members of the UK Materials Chemistry Consortium PIPE and DJC also thank the EPRSC (EP/L000202) and the UK HPC national resource, Archer, as well as the Huddersfield High Performance Computing Research Group and the STFC Hartree Centre, for computational recourses utilised in this work. We also thank to Dr Isabelle Dixon (Université Paul Sabatier, Toulouse, France) for informative discussions.

Experimental Section

The starting material [Ru(*p*-cymene)(pytz)Cl][PF_6][41] and the ligands pytz[41] and btz[33,48] were prepared by methods previously reported. Caution should be taken in the preparation of triazole-containing compounds using organic azide starting materials as these precursors are potentially explosive. C-atom to N-atom ratios of 2.5:1 to 3:1 are recommended to mitigate this risk if the azide is to be isolated prior to use rather than prepared and used *in situ*. All reagents were purchased from Sigma-Aldrich, Fluorochem and Acros Organics and were used as supplied. NMR spectra were recorded on a Bruker Ascend 400 MHz spectrometer,

with all chemical shifts being quoted in ppm referenced relative to the residual solvent signal (MeCN, δ 1.94). High resolution mass spectrometry was performed on an Agilent 6210 TOF instrument with a dual ESI source. UV-visible absorption spectra were recorded on an Agilent Cary 60 spectrophotometer. Cyclic voltammograms were measured using an Autolab PGSTAT100N potentiostat with NOVA electrochemical software. Analyte solutions were prepared using nitrogen saturated dry dichloromethane, freshly distilled from CaH_2. All measurements were conducted at room temperature under a stream of dry nitrogen at potential scan rates ranging from 50 to 500 mVs^{-1}. NBu_4PF_6 was used as a supporting electrolyte, being recrystallised from ethanol and oven dried prior to use, with a typical solution concentration of 0.2 mol dm^{-3}. The working electrode was a platinum disc, with platinum wire utilised as the counter electrode. The reference electrode was Ag/AgCl, being chemically isolated from the analyte solution by an electrolyte containing bridge tube tipped with a porous frit. Ferrocene was employed as an internal reference, with all potentials quoted relative to the Fc^+/Fc couple.

*Synthesis of [Ru(pytz)(btz)$_2$][PF$_6$]$_2$ (**1**)*

[Ru(*p*-cymene)(pytz)Cl][PF_6] (200 mg, 0.306 mmol), btz (193 mg, 0.610 mmol) and excess $NaPF_6$ (211 mg, 1.25 mmol) were added to 3:1 (v/v) EtOH/H_2O (25 mL) and heated to 90 ^oC under an N_2 atmosphere in the dark for 23 hours. The clear, pale yellow-coloured solution was then allowed to cool slowly to room temperature. The product was obtained as a yellow coloured precipitate which was collected by filtration, washed with Et_2O and dried under suction. Yield = 319 mg, 83 %.

^{1}H NMR (d_3-MeCN, 400 MHz): 5.53 (br s, 6H, C*H*$_2$), 5.56 (s, 2H, C*H*$_2$), 5.58 (s, 2H, C*H*$_2$), 7.10-7.41 (m, 26H, Ph-C*H*, Py-C*H*), 7.86 (d, *J* = 5.52 Hz 1H, Py-C*H*), 7.95 (t, *J* = 7.7 Hz, 1H, Py-C*H*), 8.02 (d, *J* = 7.8 Hz, 1H, Py-C*H*), 8.34 (s, 1H, C*H*N$_3$), 8.35 (br s, 2H, C*H*N$_3$), 8.36 (s, 1H, C*H*N$_3$), 8.66 (s, 1H, C*H*N$_3$). ^{13}C NMR (d_3-MeCN, 101 MHz): 56.01, 56.04, 56.07, 56.23, 56.27, 122.69, 123.52, 123.59, 123.70, 124.02, 125.68, 125.82, 128.60, 128.64, 128.82, 129.01, 129.71, 129.73, 129.82, 129.84, 129.91, 129.93, 129.94, 129.96, 130.00, 134.80, 134.98, 135.12, 135.14, 138.84, 141.63, 141.66, 141.71, 141.93, 149.41, 152.50, 153.68. HRMS (ES); m/z calc. for $[RuC_{50}H_{44}N_{16}]^{2+}$: 485.1486, found: 485.1491.

X-ray crystallography

Single crystal X-Ray diffraction data were collected on a Bruker D8 Venture diffractometer equipped with graphite monochromated Mo(K_α) 0.071073 nm ([Ru(*p*-cymene)(pytz)(Cl)]PF_6) and Cu(K_α) 1.54178 nm (**1**) radiation sources and a cold stream of N_2 gas. Summarised crystal and refinement data are presented in Table 2. Preliminary scans were employed to assess the crystal quality, lattice symmetry, ideal exposure time *etc*. prior to collecting a full sphere of diffraction intensity data using SMART[49] operating software. Intensities were integrated from several series of exposures, merged and corrected for Lorentz and polarisation effects using SAINT[50] software. Solutions were generated by conventional Patterson heavy atom or direct methods and refined by full-matrix non-linear least squares on F^2 using SHELXS-97 and SHELXL[51] software respectively. Empirical absorption corrections were applied based on multiple and symmetry-equivalent measurements using SADABS.[52] All structures were refined until convergence (max shift/esd <0.01) and in each case, the final Fourier difference map showed no chemically sensible features. The structure for **1** contained both a disordered hexafluorophosphate anion and a phenyl ring and these were modelled in two positions using the *PART* instruction. For all the disordered atoms the *DELU*, *SIMU* and in some cases *ISOR* constraints were used in the least-squares refinement.

Table 2. X-Ray crystallographic data for [Ru(*p*-cymene)(pytz)Cl][PF_6].MeCN and **1**.

	[Ru(*p*-cymene)(pytz)Cl][PF_6].MeCN	[Ru(pytz)(btz)$_2$][PF_6]$_2$
Formula	$C_{26}H_{29}ClF_6N_5PRu$	$(C_{50}H_{44}F_{12}N_{16}P_2Ru)_2$
M_r/g mol^{-1}	693.03	2520.04
Temperature/K	150	293
Space Group	P-1	P-1
a/Å	10.4741(6)	12.3371(5)
b/Å	11.0072(6)	21.0567(8)
c/Å	13.5855(8)	21.0921(8)
α/°	113.0580(13)	94.420(2)
β/°	96.0134(17)	90.870(2)
γ/°	100.7043(15)	100.753(2)
V/Å^3	1388.51(14)	5364.6(4)
D_x/g cm^{-3}	1.658	1.560
Z	2	2
μ/mm^{-1}	0.785	3.767
$2\theta_{max}$	64.062	144.76
N_{ref}	9667	20889
R_1	0.0481	0.0834
wR_2	0.0931	0.2311
S	1.005	1.034

Computational Details. The singlet ground state geometry of **1** was optimised using SCF procedures at the B3LYP level of theory in the gas phase using the NWChem 6.3 software package.[53] The Stuttgart-Dresden relativistic small-core ECP was used for ruthenium and 6-311G* basis sets were used for all other atoms.[54,55] The optimised minimum was confirmed through a vibrational frequency calculation. Molecular structures and molecular orbital plots were visualised using the ECCE software package. Vertical singlet and triplet state excitation energies for **1** were calculated by a TDDFT calculation at the ground state geometry. The lowest lying triplet state at the optimised ground state geometry was calculated in a single-point calculation using SCF procedures using a spin multiplicity constraint of 3. Higher lying triplet states were then determined by a TDDFT calculation starting from this triplet state wavefunction. The lowest lying triplet state was then optimised using SCF procedures by using the constraint of a spin multiplicity of 3.

Electronic Supplementary Information

Crystallographic information files (CCDC 1425928 & 1425929), electrochemical data, mass spectrometry data, optimised geometry coordinates for S_0 and T_1 states of **1** and molecular orbital plots for the ground state of **1**.

References

(1) Balzani, V.; Ceroni, P.; Juris, A. *Photochemistry and Photophysics: Concepts, Research, Applications*; Wiley-VCH, 2014.

(2) Eckenhoff, W. T.; Eisenberg, R. *Dalton Trans.* **2012**, *41*, 13004.

(3) Hagfeldt, A.; Boschloo, G.; Sun, L.; Kloo, L.; Pettersson, H. *Chem. Rev.* **2010**, *110*, 6595.

(4) Costa, R. D.; Ortí, E.; Bolink, H. J. *Pure and Applied Chemistry* **2011**, *83*, 2115.

(5) Evans, R. C.; Douglas, P.; Winscom, C. J. *Coord. Chem. Rev.* **2006**, *250*, 2093.

(6) Panigati, M.; Mauro, M.; Donghi, D.; Mercandelli, P.; Mussini, P.; De Cola, L.; D'Alfonso, G. *Coord. Chem. Rev.* **2012**, *256*, 1621.

(7) Williams, J. A. G. *Chem. Soc. Rev.* **2009**, *38*, 1783.

(8) Yersin, H.; Rausch, A. F.; Czerwieniec, R.; Hofbeck, T.; Fischer, T. *Coord. Chem. Rev.* **2011**, *255*, 2622.

(9) Bignozzi, C. A.; Argazzi, R.; Boaretto, R.; Busatto, E.; Carli, S.; Ronconi, F.; Caramori, S. *Coord. Chem. Rev.* **2013**, *257*, 1472.

(10) Zanoni, K. P. S.; Coppo, R. L.; Amaral, R. C.; Murakami Iha, N. Y. *Dalton Trans.* **2015**, *44*, 14559.

(11) Durham, B.; Caspar, J. V.; Nagle, J. K.; Meyer, T. J. *J. Am. Chem. Soc.* **1982**, *104*, 4803.

(12) Juris, A.; Balzani, V.; Barigelletti, F.; Campagna, S.; Belser, P.; Vonzelewsky, A. *Coord. Chem. Rev.* **1988**, *84*, 85.

(13) Vanhouten, J.; Watts, R. J. *J. Am. Chem. Soc.* **1976**, *98*, 4853.

(14) Garner, R. N.; Gallucci, J. C.; Dunbar, K. R.; Turro, C. *Inorg. Chem.* **2011**, *50*, 9213.

(15) Garner, R. N.; Joyce, L. E.; Turro, C. *Inorg. Chem.* **2011**, *50*, 4384.

(16) Howerton, B. S.; Heidary, D. K.; Glazer, E. C. *J. Am. Chem. Soc.* **2012**, *134*, 8324.

(17) Askes, S. H. C.; Bahreman, A.; Bonnet, S. *Angew. Chem. Int. Ed.* **2014**, *53*, 1029.

(18) Schäfer, C.; Ragazzon, G.; Colasson, B.; Larosa, M.; Silvi, S.; Credi, A. *ChemistryOpen* **2016**, *5*, 120.

(19) Baranoff, E.; Collin, J. P.; Furusho, J.; Furusho, Y.; Laemmel, A. C.; Sauvage, J. P. *Inorg. Chem.* **2002**, *41*, 1215.

(20) Collin, J. P.; Jouvenot, D.; Koizumi, M.; Sauvage, J. P. *Inorg. Chem.* **2005**, *44*, 4693.

(21) Collin, J. P.; Sauvage, J. P. *Inorg. Chem.* **1986**, *25*, 135.

(22) Fanni, S.; Keyes, T. E.; O'Connor, C. M.; Hughes, H.; Wang, R. Y.; Vos, J. G. *Coord. Chem. Rev.* **2000**, *208*, 77.

(23) Fanni, S.; Weldon, F. M.; Hammarstrom, L.; Mukhtar, E.; Browne, W. R.; Keyes, T. E.; Vos, J. G. *Eur. J. Inorg. Chem.* **2001**, 529.

(24) Sun, Q.; Mosquera-Vazquez, S.; Suffren, Y.; Hankache, J.; Amstutz, N.; Daku, L. M. L.; Vauthey, E.; Hauser, A. *Coord. Chem. Rev.* **2015**, *282-283*, 87.

(25) Sun, Q.; Mosquera-Vazquez, S.; Daku, L. M. L.; Guénée, L.; Goodwin, H. A.; Vauthey, E.; Hauser, A. *J. Am. Chem. Soc.* **2013**, *135*, 13660−13663.

(26) Welby, C. E.; Armitage, G. K.; Bartley, H.; Sinopoli, A.; Uppal, B. S.; Elliott, P. I. P. *Photochem. Photobiol. Sci.* **2014**, *13*, 735.

(27) Welby, C. E.; Armitage, G. K.; Bartley, H.; Wilkinson, A.; Sinopoli, A.; Uppal, B. S.; Rice, C. R.; Elliott, P. I. P. *Chem. - Eur. J.* **2014**, *20*, 8467.

(28) Welby, C. E.; Rice, C. R.; Elliott, P. I. P. *Angew. Chem. Int. Ed.* **2013**, *52*, 10826.

(29) Lo, W. K. C.; Huff, G. S.; Cubanski, J. R.; Kennedy, A. D. W.; McAdam, C. J.; McMorran, D. A.; Gordon, K. C.; Crowley, J. D. *Inorg. Chem.* **2015**, *54*, 1572.

(30) Mattiuzzi, A.; Jabin, I.; Moucheron, C.; Kirsch-De Mesmaeker, A. *Dalton Trans.* **2011**, *40*, 7395.

(31) Weisser, F.; Plebst, S.; Hohloch, S.; Van Der Meer, M.; Manck, S.; Führer, F.; Radtke, V.; Leichnitz, D.; Sarkar, B. *Inorg. Chem.* **2015**, *54*, 4621.

(32) Donato, L.; Abel, P.; Zysman-Colman, E. *Dalton Trans.* **2013**, *42*, 8402.

(33) Welby, C. E.; Grkinic, S.; Zahid, A.; Uppal, B. S.; Gibson, E. A.; Rice, C. R.; Elliott, P. I. P. *Dalton Trans.* **2012**, *41*, 7637.

(34) Fletcher, J. T.; Bumgarner, B. J.; Engels, N. D.; Skoglund, D. A. *Organometallics* **2008**, *27*, 5430.

(35) Monkowius, U.; Ritter, S.; Konig, B.; Zabel, M.; Yersin, H. *Eur. J. Inorg. Chem.* **2007**, 4597.

(36) Arakawa, R.; Abe, K.; Abura, T.; Nakabayashi, Y. *Bull. Chem. Soc. Jpn.* **2002**, *75*, 1983.

(37) Arakawa, R.; Jian, L.; Yoshimura, A.; Nozaki, K.; Ohno, T.; Doe, H.; Matsuo, T. *Inorg. Chem.* **1995**, *34*, 3874.

(38) Arakawa, R.; Mimura, S.; Matsubayashi, G.; Matsuo, T. *Inorg. Chem.* **1996**, *35*, 5725.

(39) Arakawa, R.; Tachiyashiki, S.; Matsuo, T. *Anal. Chem.* **1995**, *67*, 4133.

(40) Tachiyashiki, S.; Ikezawa, H.; Mizumachi, K. *Inorg. Chem.* **1994**, *33*, 623.

(41) Uppal, B. S.; Zahid, A.; Elliott, P. I. P. *Eur. J. Inorg. Chem.* **2013**, 2571.

(42) Welby, C. E.; Gilmartin, L.; Marriott, R. R.; Zahid, A.; Rice, C. R.; Gibson, E. A.; Elliott, P. I. P. *Dalton Trans.* **2013**, *42*, 13527.

(43) Li, A.; White, J. K.; Arora, K.; Herroon, M. K.; Martin, P. D.; Schlegel, H. B.; Podgorski, I.; Turro, C.; Kodanko, J. J. *Inorg. Chem.* **2016**, *55*, 10−12.

(44) Weisser, F.; Plebst, S.; Hohloch, S.; van der Meer, M.; Manck, S.; Führer, F.; Radtke, V.; Leichnitz, D.; Sarkar, B. *Inorg. Chem.* **2015**, *54*, 4621−4635.

(45) Alary, F.; Boggio-Pasqua, M.; Heully, J.-L.; Marsden, C. J.; Vicendo, P. *Inorg. Chem.* **2008**, *47*, 5259.

(46) Alary, F.; Heully, J. L.; Bijeire, L.; Vicendo, P. *Inorg. Chem.* **2007**, *46*, 3154.

(47) Klamt, A.; Schuurmann, G. *J. Chem. Soc., Perkin Trans. 2* **1993**, 799.

(48) Guisado-Barrios, G.; Bouffard, J.; Donnadieu, B.; Bertrand, G. *Organometallics* **2011**, *30*, 6017.

(49) SMART Diffracometer Control Software, Bruker Analytical X-ray Instruments Inc., Madison, WI, 1998.

(50) SAINT Integration Software, Siemens Analytical X-ray Instruments Inc., Madison, WI, 1994.

(51) SHELXTL Program System, Vers 5.1, Bruker Analytical X-ray Instruments Inc., Madison, WI, 1998.

(52) Sheldrick, G. M. SADABS: A Program for Absorption Correction with Siemens SMART System, University of Gottingen, Germany, 1996.

(53) Valiev, M.; Bylaska, E. J.; Govind, N.; Kowalski, K.; Straatsma, T. P.; van Dam, H. J. J.; Wang, D.; Nieplocha, J.; Apra, E.; Windus, T. L.; de Jong, W. A. *Comput. Phys. Commun.* **2010**, *181*, 1477.

(54) Krishnan, R.; Binkley, J. S.; Seeger, R.; Pople, J. A. *J. Chem. Phys.* **1980**, *72*, 650.

(55) Stephens, P. J.; Devlin, F. J.; Chabalowski, C. F.; Frisch, M. J. *J. Phys. Chem.* **1994**, *98*, 11623.

For Table of Contents only

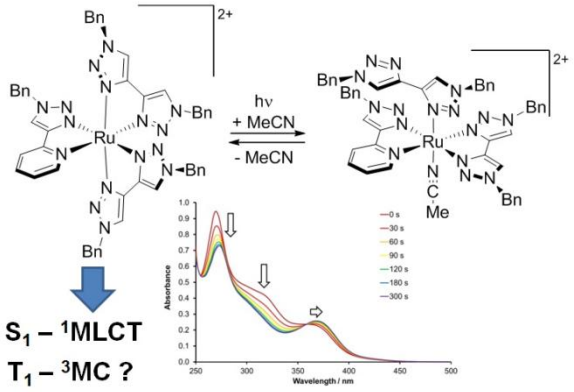

The complex $[Ru(pytz)(btz)_2]^{2+}$ (pytz = pyridyltriazole) undergoes photochemical ligand loss involving initial conversion to form a metastable ligand-loss intermediate with a monodentate bitriazolyl (btz) ligand. Computational studies suggest that whilst the S_1 state has MLCT character that the T_1 state may be MC in nature.